Optimization of Efficient Dual Band PIFA System for MIMO Half-Duplex 4G/LTE and Full-Duplex 5G Communications

MOHAMMAD A. FAKIH[1,2]**, ALIOU DIALLO**[1]**, PHILIPPE LE THUC**[1]**, (Member, IEEE),**
ROBERT STARAJ[1]**, (Member, IEEE), OUMAR MOURAD**[2]**, AND**
ELIAS A. RACHID[2]**, (Senior Member, IEEE)**
[1]Laboratory of Electronics, Antennas, and Télécommunications, CNRS, University of Nice Sophia-Antipolis, 06903 Sophia Antipolis, France
[2]CINET, Ecole Supérieure d'Ingénieurs de Beyrouth, Université Saint-Joseph, Beirut 1107 2050, Lebanon

Corresponding author: Mohammad A. Fakih (mohammad.a.fakih@gmail.com)

ABSTRACT In this paper, a two efficient Planar Inverted-F Antenna (PIFA) system for dual-band functionality on fourth-generation (4G) band (2.5-2.7 GHz) and future fifth-generation (5G) band (3.4-3.8 GHz) is presented. During the optimization process, in order to obtain an efficient system, particular attention has been paid to the antenna system efficiency as well as the isolation between the antennas. Thus, the influence of the antenna slot design used to achieve a dual-band behavior on the antenna efficiency has been particularly studied. Moreover, the antenna positions on the Printed Circuit Board (PCB) have been chosen thanks to the use of characteristic mode analysis to obtain high isolation levels in both bands. The final system is optimized for Multiple Input Multiple Output Half Duplex (MIMO HD) 4G communications and Tx/Rx Full-Duplex (FD) 5G communications. A prototype with 140 mm × 70 mm ground plane was simulated, fabricated and measured. A high isolation level between the two ports of the PIFA elements, better than 35 dB in 5G band and 20 dB in 4G band in simulation and measurement that were done in free space, is obtained. Additionally, the most important diversity metrics are computed to evaluate the potential of this two-antenna system for diversity applications.

INDEX TERMS Full-duplex (FD), half duplex (HD), isolation, multiple input multiple output (MIMO), planar inverted-F antenna (PIFA), multi-band antenna system.

I. INTRODUCTION

Multimode mobile terminals are always occupying massive interests in global wireless communication researches as for each time a new generation arrives [1]. This is due to the rapid development of the radio access technologies, where the wireless communication networks are exploiting heterogeneous networks accessing 2 or more functioning modes simultaneously, e.g. Wi-Fi and GSM, or complementary, e.g. fourth and fifth generations of mobile communications (4G and 5G). As a result, the study of multiband antenna systems became a must for present and future mobile terminals, especially concerning Multi-Input-Multi-Output (MIMO) technology [2]. Nowadays, daily speech about the emersion of 5G is extensively increasing. The reason behind this, is the necessity to increase the capacity of the channel to accommodate as much users as possible, quenching the enormous data traffic increase thirst [3] while the world is moving straightforward to enable Internet of Things ''IoT'' [4], and to lower the communication lag to less than millisecond [3]. And much more than the previous generations of wireless technology, 5G is intended to dramatically enhance the speed and volume of data transfer. This will allow users to flip through high-quality video content on mobile devices, including 4K, 3D, and virtual reality content, and have the same or better experience as watching cable television. However, the transition from 4G to 5G will not occur radically, but smoothly. So, and as the previous development of mobile technology generations, the idea of multi-mode mobile terminals came into view again. The need now is antenna systems dedicated to mobile terminals that may support, the 4G/LTE and the 5G bands at the same time [2]. Several different operating frequencies for the 5G technology, are under negotiation including the 28 GHz, 38 GHz, 60 GHz, and even in the

The associate editor coordinating the review of this manuscript and approving it for publication was Luyu Zhao.

sub-6 GHz, (3.4-3.8 GHz) [5]–[9]. Thus, different works have considered the sub-6 GHz band as an important candidate for 5G communications [10]–[12]. One of the key features of 5G is to exploit the Full-Duplex (FD) technology [13], [14]. FD radio technology has attracted significant research attention to introduce a new communication model, where the same carrier frequency is deployed for concurrent transmission and reception at the same user equipment or base station [13]. Theoretically, it is doubling the system throughput over conventional HD MIMO while requiring no additional bandwidth [14], [15]. But, in order to have good performance FD systems need to deal carefully with the self-interference (SI) issue, i.e., the interference caused by the transmitting antenna to the receiving one if they are close to each other. Recent results show that SI can be reduced for about 100 dB as in [16], and this can be sufficient for realizing the FD technology. However, this isolation level is reached by adding the effect of 3 types of SI cancellation solutions called, *analog cancellation technique, digital cancellation technique, and field cancellation technique* [14], [15]. If we consider antenna systems for MIMO or FD applications, the field cancellation technique corresponds to the improvement of the isolation between closely spaced antennas. This can be obtained by the use of different decoupling techniques such as decoupling networks [17], neutralization lines [18], quarter wavelength filter [19], introduction of some well-designed slots into the ground plane in case of mobile terminals [20], and additional local ground plane [21]. Usually, these solutions lead to improve the isolation level of about 20 dB which is sufficient for HD MIMO applications but insufficient for FD ones which need a minimum isolation level of 100 dB as aforementioned. Other solutions could be the use of metamaterials [22] where its usage may cause radiation efficiency drops [23], or the defected ground structure (DGS) [24], which is not at all realistic for mobile telephony where the screen itself can be considered as a metallic plane that removes the effect of the DGS [25]. Moreover, all these techniques are considered narrow band which is not the case in the 5G band. Therefore, exploiting characteristics modes of the Printed Circuit Board (PCB) by finding the optimal positions of the 2 antennas to obtain the maximum isolation has been also used [26]–[29]. This solution is interesting although the isolation level reached is not sufficient for our purpose.

In this work, the design of an antenna system for compact size mobile terminals (MTs), powered for dual-band 4G HD MIMO and 5G FD capabilities is presented. To achieve the required isolation (at least of 20 dB) for HD technology and quite high isolation (at least of 35 dB) for FD technology, the field type cancellation of SI signals resulting from closely spaced antennas on the same MT PCB is only used and studied. This isolation level may be improved by the 2 other types of SI cancellation techniques (analog and digital) to reach the minimum isolation level of 100 dB needed for FD systems. This paper is organized as follow, in section II, a single dual-band PIFA (Planar Inverted-F Antenna) covering the LTE

band (2.5-2.7 GHz), for 4G communications and the sub 6 GHz band (3.4-3.8 GHz) for 5G communications thanks to the use of slot is presented. In the same section, the effect of slot positioning over the antenna element on its efficiency is investigated, where up to our best knowledge, no previous studies have addressed this issue. In Section III, the integration of a second identical antenna on the same small PCB in order to obtain at the same time a 2×2 HD MIMO for 4G and Tx/Rx FD for 5G system is described. Particular attention was brought to find the antenna positions allowing to achieve the best isolation levels, thanks to the use of the characteristic mode study. This later (based on the Characteristic Modes Theory) can give rapidly the positions where antennas should be placed to have high isolation even without using other isolation enhancing methods. Moreover, a prototype of the optimized system was fabricated and its overall performance was measured and compared with simulated results obtained with ANSYS HFSS software in order to validate our proposed solution. In Section IV, the diversity characterization of MIMO HD 4G antennas is studied. Section V concludes the paper.

II. OPTIMIZATION OF THE DUAL-BAND PIFA

When researchers and developers are interested in designing compact size MTs, small antennas with low and small profile structures are a prerequisite [30]. Monopoles and PIFAs are excellent candidates for this mission, because of their great abilities and feasibilities to have good results in all terms of antenna parameters, matching, and radiation. This work will focus mainly on PIFA since it is a better solution to obtain dual-band functionality without effectively losing other antenna features and characteristics.

For this study, a metallic ground plane having the real size of a smartphone, 140 mm × 70 mm is chosen. The starting design was a simple PIFA optimized to operate in low-frequency band dedicated for the 4G communications (2.5-2.7 GHz), with 2.6 GHz as resonant frequency. Its size was calculated from [30] using the equation:

$$L_{PIFA} + W_{PIFA} + H_{PIFA} - W_{short} = \lambda/4 \qquad (1)$$

where L_{PIFA} is the PIFA length, W_{PIFA} is its width, H_{PIFA} is the height and W_{short} is the width of the shorting pin. The PIFA is positioned at 4 mm × 3 mm from the upper corner of the ground plane and its height was set to 7.7 mm. This height is suitable for nowadays MTs as shown in [31]–[35] where their thickness is higher than 8 mm. After optimization, the antenna dimensions were found to be $L_{PIFA} = 21$ mm, and $W_{PIFA} = 11$ mm. The width of the feed and the short pins are both equal to 1mm. The material used to design our PIFA is nickel silver (Cu, Ni, Zn) of conductivity 4×10^6 S/m, and its thickness is 0.3 mm. Figure 1 shows the complete design.

The model is simulated over HFSS, and the result in terms of the reflection coefficient is shown in Figure 2 where the two first expected resonance modes of the PIFA are well observed. The resonance frequencies are 2.6 GHz and 6.22 GHz. Focusing on the desired band (2.5-2.7 GHz),
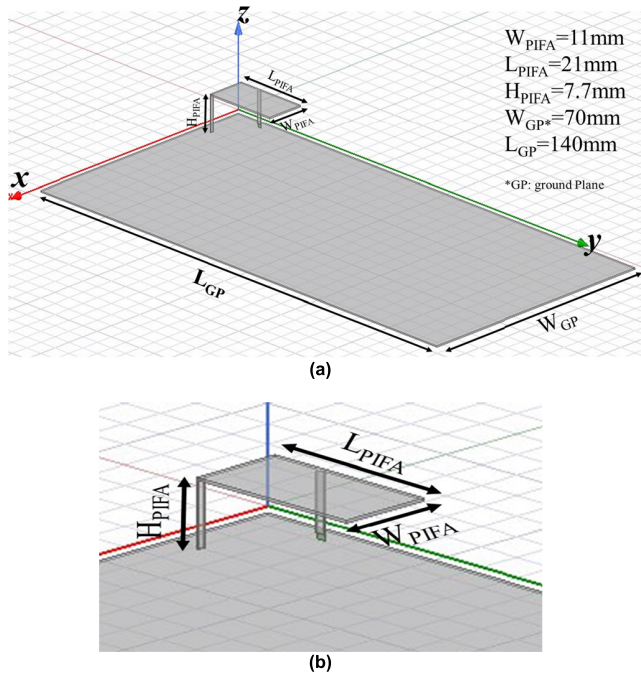
$W_{PIFA}=11mm$
$L_{PIFA}=21mm$
$H_{PIFA}=7.7mm$
$W_{GP*}=70mm$
$L_{GP}=140mm$

*GP: ground Plane

(a)

(b)

FIGURE 1. PIFA antenna with its MT ground plane: (a) whole System and (b) zoom over PIFA radiating element.
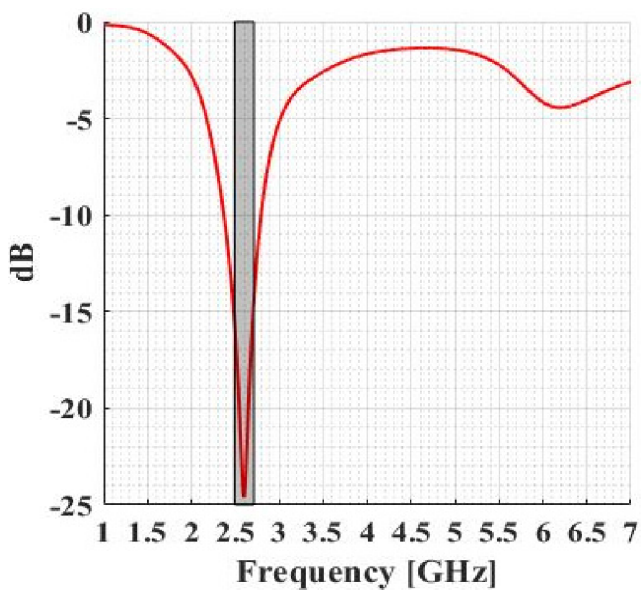

FIGURE 2. Simulated reflection coefficient of the PIFA.

the covered bandwidth of 430 MHz (ranging from 2.37 GHz to 2.8 GHz) is obtained for a matching criterion of reflection coefficient less than −10 dB.

The second step consists in achieving the dual-band functionality, to cover the desired higher frequency band allocated for 5G communications (3.4-3.8 GHz). For this aim, slotting technique over the PIFA plate is applied, in order to decrease the frequency resonance of its third higher-order mode (6.22 GHz) [36]–[38]. The width of the slot, its length and its position over the plate have an important influence in the shifting process as well as on the antenna efficiency.
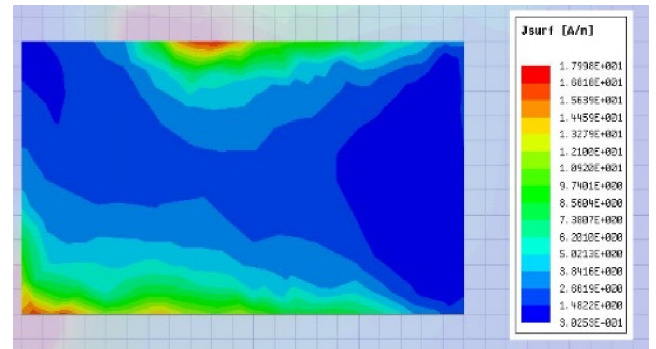

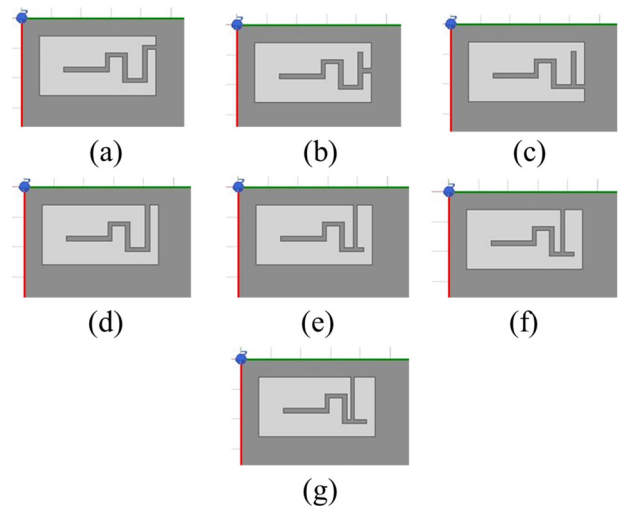**FIGURE 3.** Current distribution over the PIFA at resonance frequency of 2.6 GHz.

FIGURE 4. The seven tested configurations for slot openings over short and long edges of the PIFA.

Moreover, the slot design must not disturb the first mode of resonance in the low band allocated for 4G communications. As a result, this PIFA must be carefully slotted in the area where the current distribution is low (Figure 3), to preserve the resonance in the low desired band. Different slots with different sizes have been tested, to reach the high desired band. After optimization, the slot length and its width were fixed to 28.3mm mm and 0.7 mm respectively. The slot takes a ''snake'' shape in line with the region where the current distribution is low. The opening position of this slot was also studied. Seven different configurations as shown in Figure 4, were tested to show the effect of the slot opening position over the PIFA plate, on the antenna reflection coefficient and its radiation efficiency (η_{rad}).

To realize this study, the opening of the slot was swept on both, the short and the long edge of the PIFA, while conserving the overall size and the initial geometry of the slot and without any further modifications. Three positions were chosen for opening the slot on the short edge of the PIFA (Figures 4a to 4c). Figures 4d to 4g show the four slot opening positions along the long edge. Figure 5 compares first the simulated reflection coefficients obtained for these
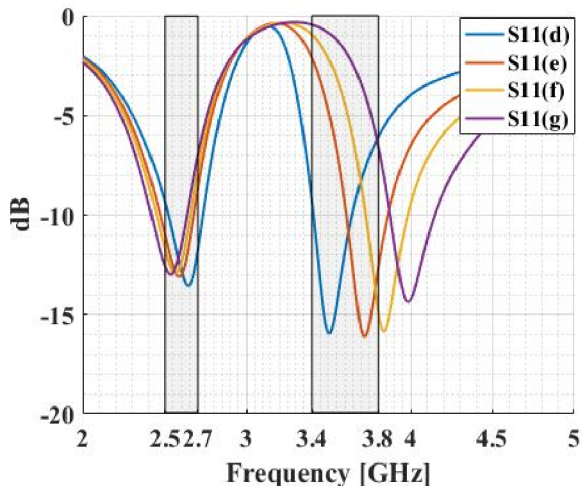
FIGURE 5. Simulated reflection coefficients for different configurations slot openings along the long edge of the PIFA.
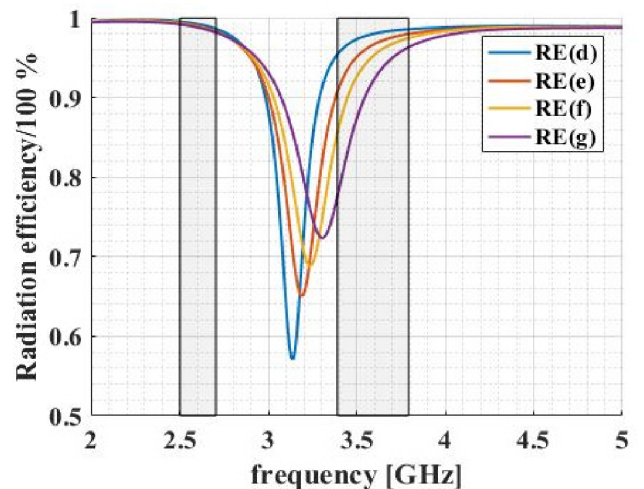

FIGURE 7. Simulated radiation efficiency (η_{rad}) for different configurations slot openings along the long edge of the PIFA.
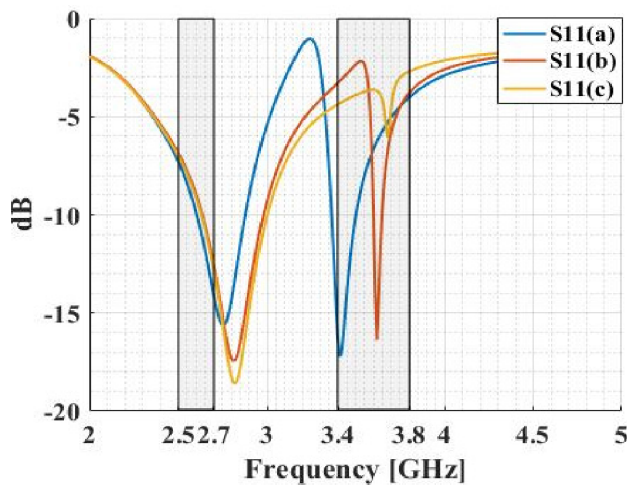

FIGURE 6. Simulated reflection coefficients for different configurations slot openings along the short edge of the PIFA.
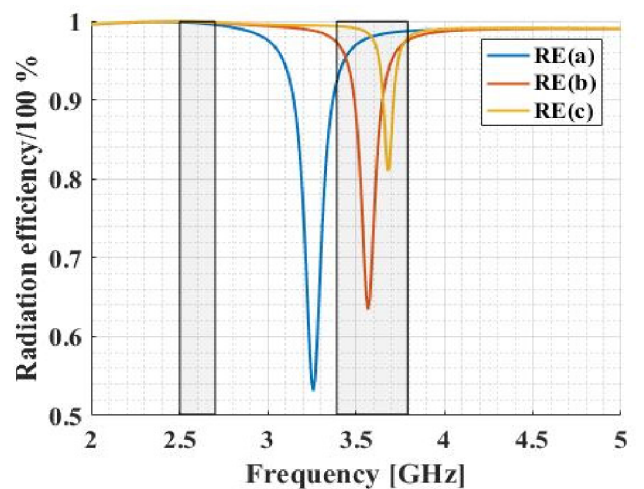

FIGURE 8. Simulated radiation efficiency (η_{rad}) for different configurations slot openings along the short edge of the PIFA.

different slots opening positions over the long edge. It is noticed that the higher bandwidth changes drastically as well as the resonant frequency in this band. However, the antenna is always matched even if it is not always in the desired band except for a specific slot opening position (case (d)). Moreover, for the lower band, the resonant frequency shifts slightly while sweeping without having a significant effect on the level of matching nor on the desired bandwidth.

The results concerning the slot opening positions over the short edge are presented in Figure 6. In the three cases, the low-frequency band shifts and is always out of the desired one. Moreover, for the higher one, although resonance always exists for all configurations, its level in terms of matching changes drastically.

The bandwidth becomes narrower and narrower in line with the slot opening position. We can observe the particular shape of the bandwidth corresponding to the slot resonance, which is placed in the high desired band, for all slot positions. Indeed, for all cases, a sharp and rapid decrease in

the reflection coefficient curves is seen. This issue leads us to study carefully the evolution of the antenna radiation efficiency at these specific frequencies versus the slot openings over both long and short edges (Figures 7 and 8). For the sweeping over the long edge, the results represented by Figure 7 show that for the low band, the behavior of the antenna radiation efficiency (cases (d) to (g)), is the same all over the band. However, it is observed that it exists a deep decrease between the high and low desired bands depending on the slot opening configuration. Indeed, for the worst-case (g), a difference of 17% is obtained between the lower and upper limits of the band (79% at 3.4 GHz instead of 96% at 3.8 GHz) respectively.

The study of η_{rad} of the short edge slot sweeping shown in Figure 8, reveals that the deep gap between the 2 bands slides significantly with the slot opening, sweeping towards the high band with a significant increase in its level. It is observed, that the η_{rad} curves case (b) and case (c) corresponding to configurations (b) and (c) of Figure 5 respectively
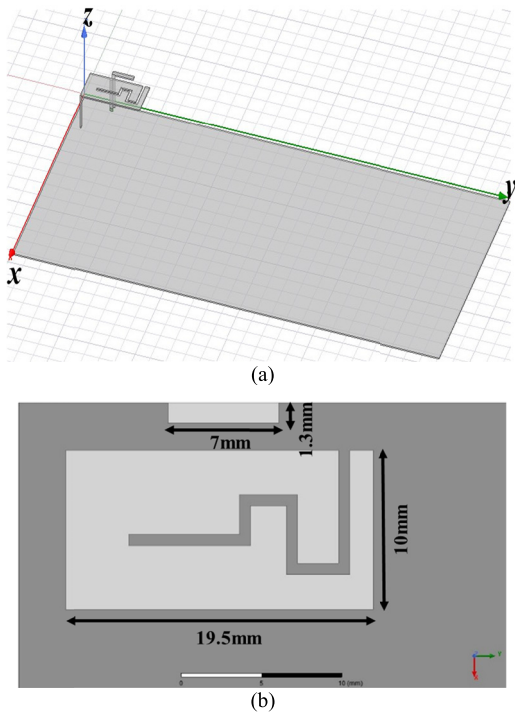
FIGURE 9. Slotted PIFA with parasitic element for dual-band functionality: (a) 3D view and (b) top view.
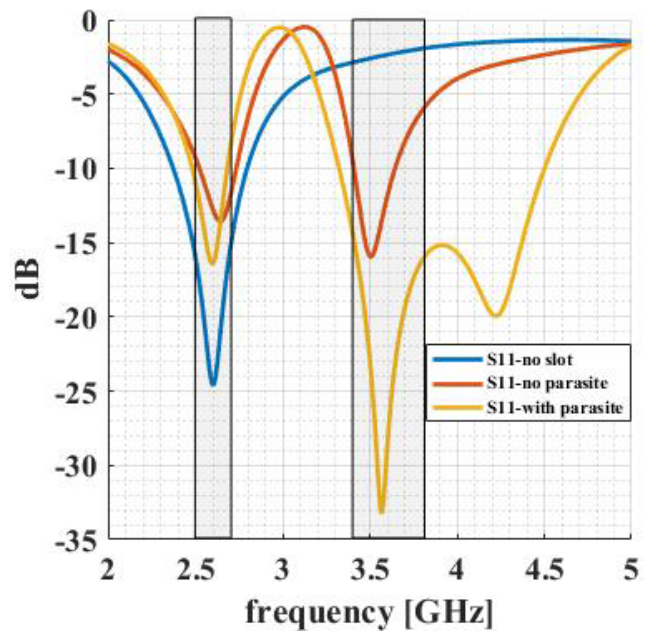

FIGURE 10. Comparison of the simulated reflection coefficients of the initial PIFA without slot and the dual-band slotted PIFA with and without parasitic element.
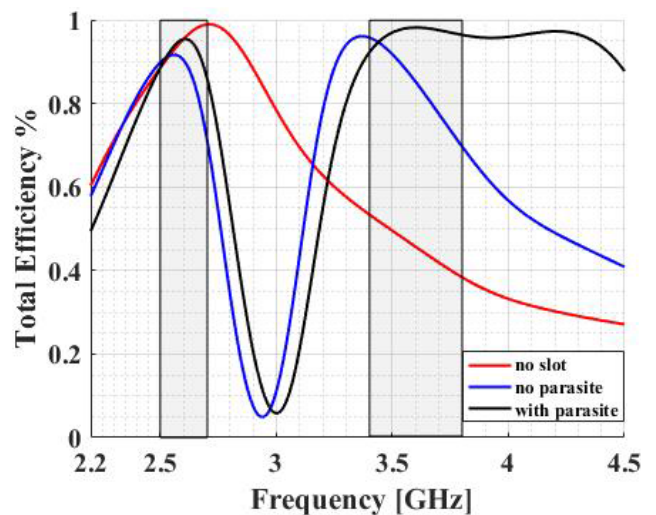

FIGURE 11. Simulated total efficiency (η_{tot}) of the single PIFA, PIFA with slot and PIFA with slot and parasitic element.

are totally included in the high desired band. As a conclusion, the slot opening position over the PIFA plate must be chosen very carefully, in order to maximize the dual-band PIFA η_{rad}. This choice may disturb the first resonance mode even when choosing the slotting over the low current distribution area of the PIFA. Therefore, the slotting technique must be carefully applied taking into account all parameters that may affect the results in terms of matching and efficiency and has to be studied more in details to define future designing rules.

Regarding the previous results, and after optimization, concerning the size and shape of the slot, configuration (d) of Figure 4 is chosen to proceed. However, the use of the slot creates only narrow bandwidth insufficient to cover the whole desired high band. Moreover, a slight shift in the low-frequency band is noticed, leading to resizing and repositioning the PIFA to 3 mm × 3 mm from the upper right corner instead of 4 mm × 3 mm as previously announced. Therefore, to enlarge the desired higher band, a second technique also used to create multi-band antennas is applied. It consists of adding a quarter wavelength parasitic element to create a new resonance [39]. Nevertheless, the choice of its size and position close to the driven element must also be carefully studied in order to remove efficiency drops which may occur with this kind of solutions [40]. After optimization done by simulation, the suitable size and position of this parasitic element to cover the whole 5G band was found (Figure 9). The new antenna dimensions are L_{PIFA} = 19.5 mm, W_{PIFA} = 10 mm, while the size of the parasitic element is 7 mm × 1.3 mm and its height is still 7.7 mm. The total size of the slot was also further optimized to be 27.8 mm and its width equal to 0.7 mm.

The simulated reflection coefficient is shown in Figure 10. It is seen that the dual-band functionality is now well obtained. The two desired bands are well covered by this configuration with parasitic element in contrary to the other two starting configurations: initial PIFA design with no slot (Figure 1) and dual-band PIFA without parasitic element (Figure 4d). The 4G band covered with the first mode of the PIFA, goes from 2.5 to 2.7 GHz at −10 dB. The 5G one starting at 3.34 GHz to 4.5 GHz at the same (−10 dB) level, is obtained by the coupling of the third mode of the PIFA and the resonance frequency of the parasitic element. Thus, for the upper band, a very wide bandwidth greater than 1 GHz
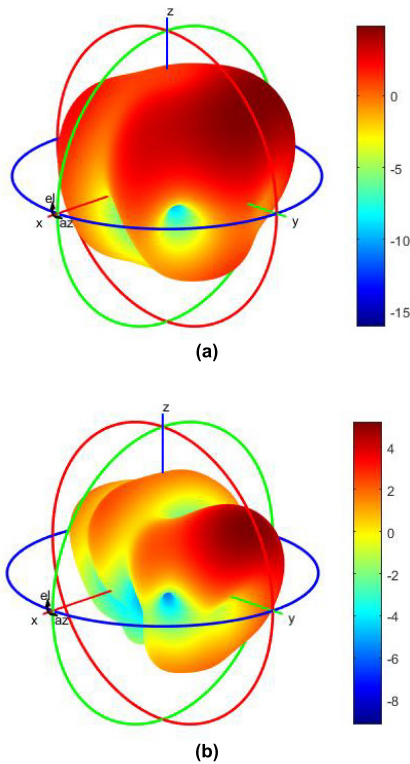
FIGURE 12. 3D radiation patterns of the slotted PIFA with parasitic element: (a) 2.6GHz and (b) 3.6GHz.

FIGURE 13. Current distribution over slotted-PIFA antenna system with parasitic element: (a) at 2.6 GHz and (b) at 3.6 GHz.

(a): Major Axis Symmetry   (b): Minor Axis Symmetry

(c): Center of Symmetry

FIGURE 14. The 3 different configurations of antennas positions over ground plane: (a) major axis symmetry, (b) minor axis symmetry, and (c) center of symmetry.

is achieved thanks to the coupling of the two resonances obtained by the uses of slot and added parasitic element.

Figure 11 shows the simulated total efficiency (η_{tot}) of the initial PIFA configuration in addition to slotted PIFA with and without parasitic element antenna systems. The η_{tot} in the 4G band ranges between 85% and up to than 99% for the initial PIFA configuration and between 85% and up to more than 90% for the other two configurations. For the dual-band PIFA, the η_{tot} obtained in the high band is between 70% and 90% without parasitic element because the 5G band is partly covered, while it is noticed that the η_{tot} is always over 90% in the whole 5G band for the structure with the parasitic element.

Figures 12a and 12b show the simulated 3D radiation patterns of the suggested dual-band PIFA antenna at 2.6 GHz and 3.6 GHz respectively. The main radiating direction is in the YOZ-plane at an angle of around 45° for both frequencies. The total gain is found to be 5.4 dBi at 2.6 GHz and 5.2 dBi at 3.6 GHz.

III. OPTIMIZATION OF THE DUAL BAND-ANTENNA SYSTEM

As aforementioned in the Introduction, adding a second antenna element on the same PCB is the next target. The radiating element chosen is another slotted PIFA having all the same dimensions as the initial one. In order to maximize η_{rad} of the antenna system, a study to obtain the best isolation level between the two radiating elements was performed by investigating different antenna positions on the PCB. In this
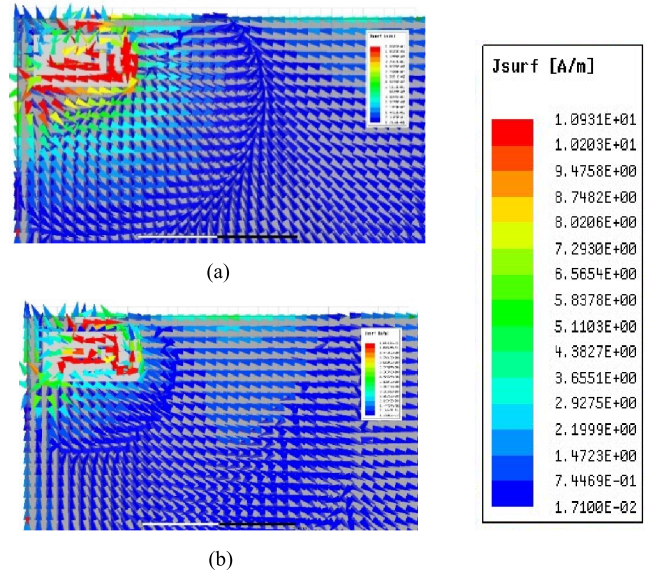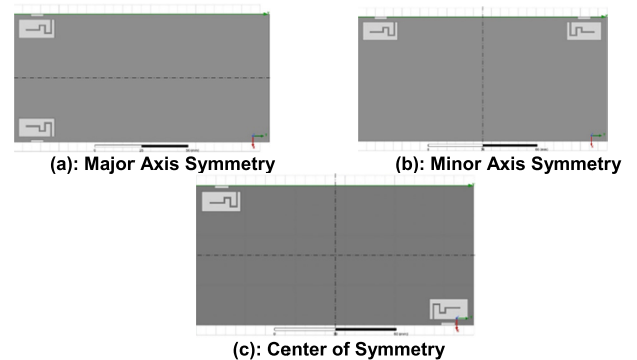
methodology, we are dealing with field interference cancellation only without taking into account the other cancellation techniques. Before adding the second dual-band PIFA on the same ground plane, the current distribution vectors of the single dual-band PIFA with parasitic element has been studied (Figure 13).

The plot at 2.6 GHz shows that the main radiating parts at this frequency are the PIFA plate and a part of the mobile chassis due to high current distribution presents in this area. At 3.6 GHz, the main radiating parts are this time the slot and the parasitic element. Then, the second antenna (ANT-2) positioned on the other corner symmetrical to the first one (ANT-1) with respect to the major axis of the PCB (**Case (a)**) is introduced (Figure 14a). Moreover, two other positions are also studied for the ANT-2: on the fourth corner symmetric with respect to the minor axis of the PCB (**Case (b)**) as shown in Figure 14b, and on the opposite corner where the maximum distance of separation between the 2 PIFAs is obtained i.e. symmetric with respect to the center of the PCB (**Case (c)**) as
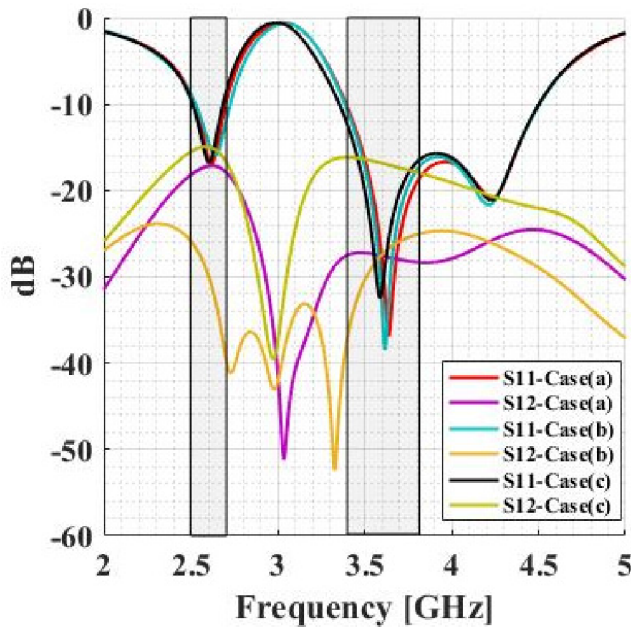
FIGURE 15. Simulated S-Parameters of the 3 different configurations.

TABLE 1. Matching and isolation levels for the three different antenna configurations in the low and high bands.

	Low desired band		High desired band	
	Match range (dB)	Isolation range (dB)	Match range (dB)	Isolation range (dB)
Case (a)	-17 to -8	18 to 17	-37 to -10	28 to 27
Case (b)	-16 to -10	17 to 15	-32 to -12	18 to 16
Case (c)	-15 to -8	40 to 25	-38 to -10	38 to 25

in Figure 14c. The simulation of the Scattering (S) parameters of these 3 different cases are represented in Figure 15. Due to structures symmetry in the three cases, S11 and S22 are coinciding as well as S12 and S21 and that is why S22 and S21 are not represented. For **Case (a)**, it is noticed that the low band is still matched as well as the high band at a level minor to −10 dB, whereas the isolation levels differ between the low band and high band. For the low desired band, it has a minimum of 17 dB and a maximum of 18 dB less than the 20 dB expected for this band to perform 4G MIMO communications. In the high band, the isolation magnitude ranges between 27.5 dB and 28.3 dB. For **Case (b)**, the simulation results show that the 2 bands are still matched as in the previous configuration, but the isolation levels are worse in the two bands. Indeed, in the low band, the isolation level is now ranging between 15 dB and 17 dB maximum for the whole desired band, whereas it is ranging between 16 dB and 17 dB for the high band. Now for **Case (c)**, the results show that the low and high bands are also still matched at −10 dB. The isolation levels are much better compared to the first two cases. For the low band, it has a minimum of 26 dB and a maximum of 39.7 dB level of isolation. This means that this position is suitable for 2 × 2 HD MIMO 4G communications. Concerning the high band, the isolation ranges between 25 dB minimum and 37 dB maximum. Table 1 summarizes the differences between the 3 configurations: (i) major axis symmetry (**Case (a)**), (ii) minor axis symmetry (**Case (b)**) and (iii) center of symmetry (**Case (c)**), in the low and high bands. As a result, and especially when comparing the first and the second cases, it is clear that high isolation level, does not depend surely on the distance between PIFA elements over ground plane.

To justify this latter observation, a new study was done on several other antenna positions over the ground plane where

better isolation levels could be obtained, even not for highest distance of separation between antenna elements. Thus, ANT-1 was fixed at the upper left corner while the ANT-2 was firstly fixed as in **Case (c)**. ANT-2 was then moved over the short and long edges seeking for better isolation level but no interesting results were found. Then, ANT-2 was fixed as in **Case (a)**. The same movement procedure was applied by moving ANT-2 from a point **A (57 mm, 3 mm)** along –X direction (distance between the edge of ANT-1 and the edge of ANT-2 of 44 mm) to a point **B (15 mm, 3 mm)** which corresponds to a 2 mm separation between the 2 antennas (edge to edge). Then, ANT-2 was moved along Y direction starting with the same point **A**, towards the third corner **F (70 mm, 140 mm)** to reach point **E (57 mm, 117 mm)** of the mobile chassis where the antenna remained 3 mm apart from the corner. This movement procedure led to interesting results in terms of isolation (Figure 16). We can see that there exist some points over the mobile chassis where we can have good isolation level for MIMO HD 4G mobile communications and, at the same time, a quite high level for the FD 5G mobile communications. The best isolation level was found for the ANT-2 at point **D (57 mm, 87 mm)** as shown in Figure 17. We can observe that ANT-1 is positioned at the upper left corner while the ANT-2, is placed over the long side at a distance of 77.9 mm (0.935λ) corner to corner, between the 2 PIFAs, where λ is the wavelength corresponding to the resonant frequency of 3.6 GHz (Figure 17). We can notice that as it is a non-symmetrical case, S11 and S22 parameters are not coinciding anymore.

Although we are not used to this form of antenna position on the edges of mobile chassis, where designers usually select the corner (top or bottom) to implement it, a change in the way of thinking is a must when we are seeking for more complicated communication system like FD system.

Furthermore, the position of the antenna over the PCB affects its resonant frequencies. Indeed, a shift of the first resonant frequency of ANT-2 which resonates now at 2.5 GHz, is observed (Figure 22). Despite this shift and due to the high band of coverage at −10 dB, the low band allocated for 4G communications is still covered by ANT-1. Concerning the band covered by ANT-2, we can observe that the bandwidth at −10 dB is narrower due to the shift of the resonance
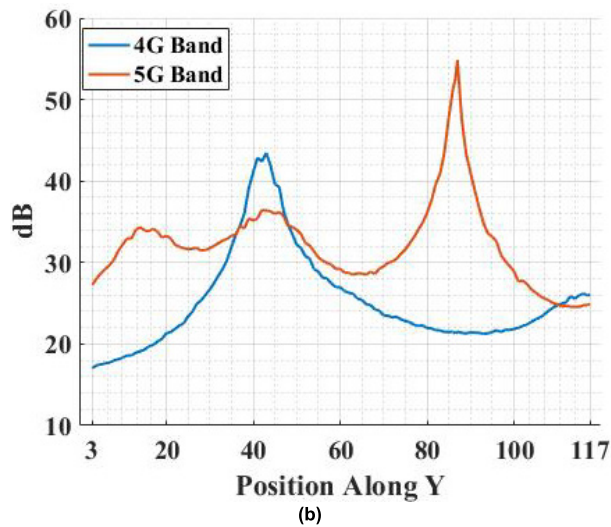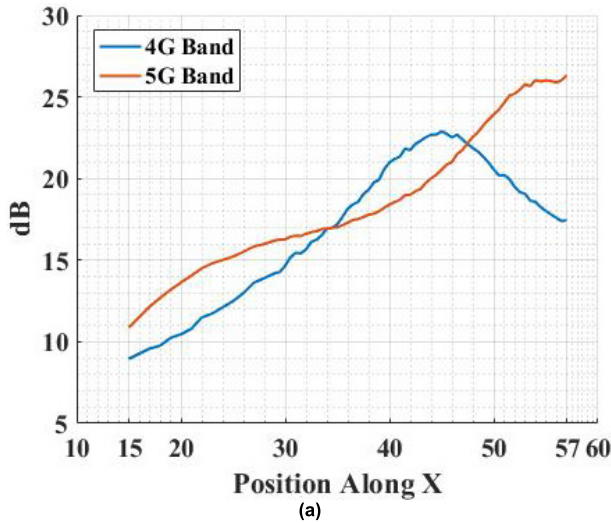
FIGURE 16. Isolation level as function of position of ANT-2: (a) along X-direction (b) along Y-direction.

FIGURE 17. Top view of antennas location for the best isolation in the high band.

frequency of the first mode of the PIFA. This loss can be recovered by resizing ANT-2. The results also show that the high band allocated for 5G communications is still totally covered by both antennas, despite a very slight shift in the resonant frequency.

Concerning the isolation, it is observed a minimum of 35 dB and up to around 54 dB in the high band where it is still having a minimum of 20 dB isolation at the same time suitable for the HD MIMO 4G application in the low band. These results where unexpected as the distance of separation between the antenna elements is not the maximum, but they confirm the previous conclusion that the highest distance of separation does not surely correspond to better isolation level.

To explain this strong isolation between the 2 antennas at these positions, we simulated the characteristic modes of the ground plane [41], [42]. It is proved that for each mobile chassis there exist several characteristic modes that can be excited to constitute together with the antenna, a radiating element [43]. T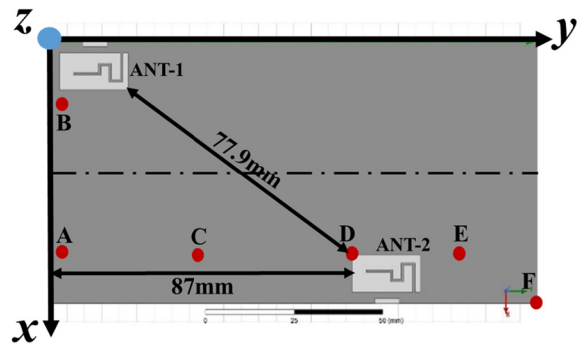hese characteristic modes can be either odd or even which are considered orthogonal modes. The advantage of these modes is that often when the current distribution shows a maximum value for a given characteristic mode in a given position of the mobile chassis, it can also show a minimum value for another orthogonal mode at the same position at the same time. This means that we are able to excite different orthogonal modes independently using appropriate antennas that can be implemented at these positions where the current is maximum for one mode while minimum for the other mode. Hence, if an antenna excites a given odd mode at a specific position, while a second antenna excites another orthogonal mode at another position, then the isolation level between the two antenna ports can be easily enhanced. Therefore, in order to improve the isolation level between two antenna ports, we have to excite two orthogonal modes independently at two different positions of the mobile chassis by means of two different antenna ports. In order to select the two desired orthogonal modes, we have to check the most significant modes that meet the following two conditions simultaneously: the characteristic significance value must be close to the 1 and the characteristic angle value must be close to 180 degrees. The simulation results of the characteristic significance (Figure 18a) and the characteristic angle (Figure 18b) show that in the high band, in addition to the odd modes (1 and 5), the even mode (2) is also radiating at 3.6 GHz meeting the two aforementioned conditions.

The observation of the characteristic currents of the odd mode 1 (Figure 19a) and the even mode 2 (Figure 19b) at 3.6 GHz shows that these 2 orthogonal modes can be excited by different positions on the ground plane. These positions correspond to those found for the 2 antennas on the PCB, which explain the strong isolation obtained.

A prototype of this configuration was fabricated (Figure 21). The S-parameters were measured with a ZVM Rohde and Schwarz Vector Network Analyzer [44] and then compared with the simulation results (Figure 22). The simulations were done in two configurations: with and without a screen aiming to check the effect of the screen on the designed antenna system. The modeled screen consists of 3 parts: metallic back, display screen, and glass. From [45] and [46], the permittivity of the glass is $\varepsilon_{glass} = 5.5$ and the OLED
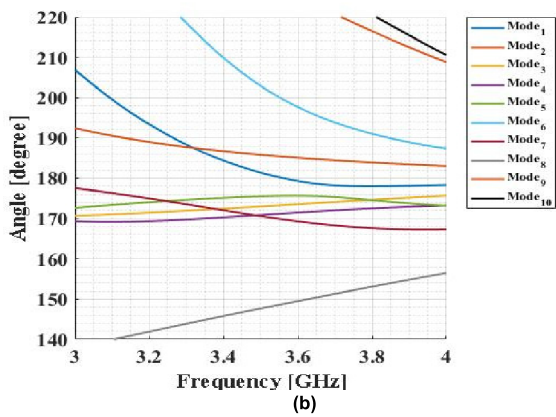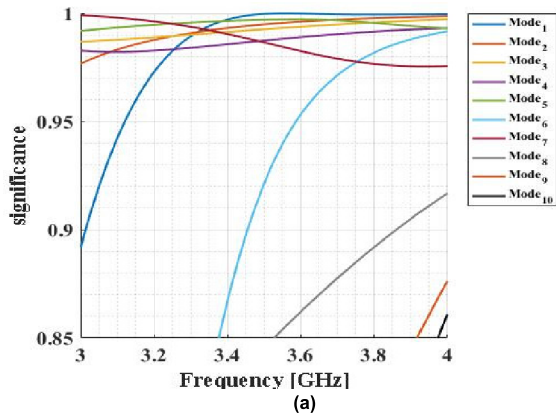
FIGURE 18. Characteristic modes of the ground plane (a) Significance. (b) Angle.
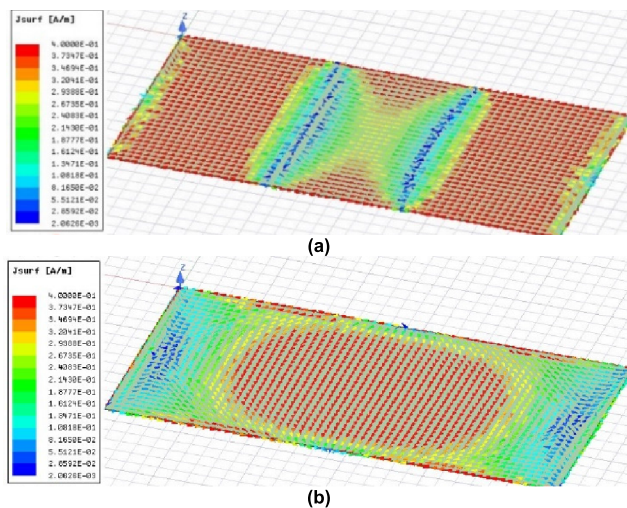

FIGURE 19. Characteristic current on the ground plane at 3.6 GHz (a) of mode 1 (b) of mode 2.

display screen is $\varepsilon_{OLED} = 3.23$. The screen was aligned back to back with the antenna system, where the metallic back touches directly the ground plane of the antenna system to constitute together one metallic plane as shown in Figure 20. The comparison between the simulated results with and without the presence of the screen shows a slight shift in the resonance frequencies while the effect on the isolation
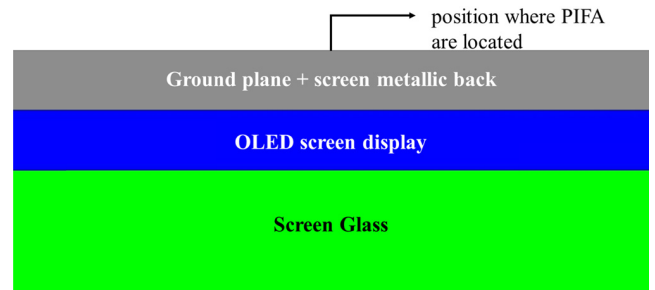

FIGURE 20. Side view of the alignment of the screen with the antenna ground plane.

FIGURE 21. Fabricated prototype of double dual-band slotted PIFAs with the best isolation between the 2 elements.

is negligible (Figure 21). The results of Figure 21 show also a good agreement between the simulated (without screen) and the measured results. The slight shifts and small differences occurred in the matching levels between simulation and measurements are mainly due to fabrication and experimental tolerances. The impurities of the used metal, as well as the cable influence [47] and difficulties in measurements, may also play a role in the differences between the simulation and measured results.

If we analyze the measurement curves of this prototype, it is shown that the 2 desired bands are totally covered, and at the same time, the minimum level of 20 dB suitable for 2×2 HD MIMO for 4G/LTE communications has been reached.

Indeed, the minimum isolation level measured for this prototype is 35 dB at the boundaries of the high desired bandwidth, which is equal to the simulation result, but it can also reach more than 65 dB in the middle of the band, as shown in Figure 22. This very good result could certainly be further improved by the application of analog and digital cancellation techniques in order to completely fulfill the isolation requirements for FD 5G communications.

Figure 23 represents the 2D simulated and measured radiation patterns in the XOZ and YOZ planes. The measurements were done in the anechoic chamber of LEAT using a KEYSIGHT PNA-X N5264A measurement machine [48]. It is shown that the measured patterns agree well with the simulated ones. The slight differences are also caused by the influence of feeding cables, as well as the fabrication tolerances and measurement difficulties [47]. The radiation pattern of each PIFA was also simulated and measured to verify the pattern diversity of the system. Figures 23a and 23b
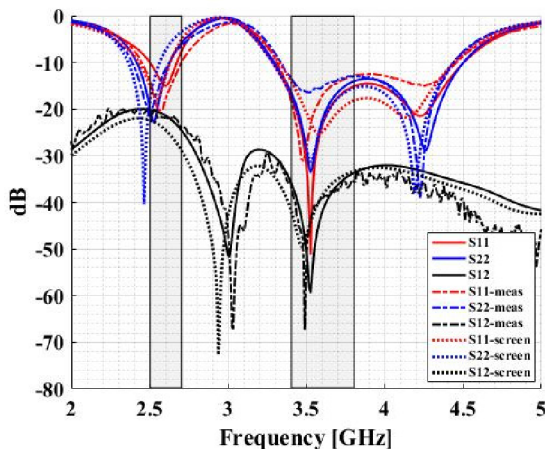
FIGURE 22. Simulated (with and without screen) and measured S parameters of the dual-band PIFA system.

FIGURE 23. Simulated and measured radiation patterns of the two-PIFA system: (a) 2.6 GHz; (b) 3.6 GHz. When ANTi is excited, ANTj is loaded by 50 Ω.

show respectively the radiation patterns at the low resonant frequency of 2.6 GHz and at the high frequency of 3.6 GHz, when alternatively, ANT-1 is excited and ANT-2 is loaded by 50 Ω and vice versa. It is also noticed from Figure 23 that when ANT-2 is excited, the radiation patterns are very different than when ANT-1 is excited, because of non-symmetric position and this may be advantageous for diversity feature. The simulated realized gain when ANT-1 is excited is found to be 5.4 dBi and 6.5 dBi while the measured ones are 5.6 dBi and 6 dBi at 2.6 GHz and 3.6 GHz respectively. When ANT-2 is excited the simulated gains are 5.7 dBi and 4.5 dBi whereas the measured total gains are 4.8 dBi and 3.9 dBi at 2.6 GHz and 3.6 GHz respectively.

The total efficiency η_{tot} was then measured in a SATIMO STARLAB 18 antenna measurement facility [49]. Figure 24 shows the comparison between the measured and simulated efficiencies of the two antennas system. We can observe that the simulated and measured results are in good agreement. η_{tot} in the low band ranges between 85% and more than 90% when ANT-1 is excited and ANT-2 loaded by 50 Ω and between 70% and up to more than 90% when ANT-2 is excited and ANT-1 loaded by 50 Ω. The η_{tot} curve of ANT-1 for the two-PIFA system is close to the one obtained with the dual-band PIFA with parasitic element of Figure 11, probably because of the same position over ground plane, as well as the high isolation level between the two antenna ports as η_{tot} is given in terms of η_{rad} and S parameters as (2).

$$\eta_{tot} = \eta_{rad}\left(1 - |S11|^2 - |S12|^2\right) \qquad (2)$$

The differences between the η_{tot} of ANT-1 and ANT-2, of the two-PIFA antenna system in the low band, are due to non-symmetric form of the system as observed by comparing S11 and S22 of Figure 22. In the high band, the η_{tot} of both antennas is between 90% and 98% upon the whole band. The measurement results show an efficiency of up to 88% but no less than 70 % for both desired bands.

If we compare these results to other similar works, in [38], to cover the bands of GSM 900 and DCS 1800, the authors used slotted PIFA techniques to attain dual-band functionality while the efficiency is not studied. In [39], the authors used in addition to the slotting PIFA technique, a parasitic element to cover GSM/PCS and GPS standards. The studied efficiency shows better values than 60% in all bands. In [50], the authors use only the slotting PIFA technique to acquire the following bands: GSM, DCS, PCS, UMTS, WiBro, Bluetooth, SDM-B, WiMax, and WLAN. The recorded efficiency was better than 79% in all the covered bands. In [51], the authors succeeded to acquire a very large bandwidth from 2 GHz and to 6 GHz suitable for WLAN applications and using ground plane etching technique, to increase the bandwidth of their designed PIFA, but unfortunately, the efficiency of the design is not given. The authors of [52], used printed IFA antenna solutions to acquire wideband suitable for GSM 1800, GSM 1900, UMTS, LTE 2300, LTE 2500 and WLAN bands.
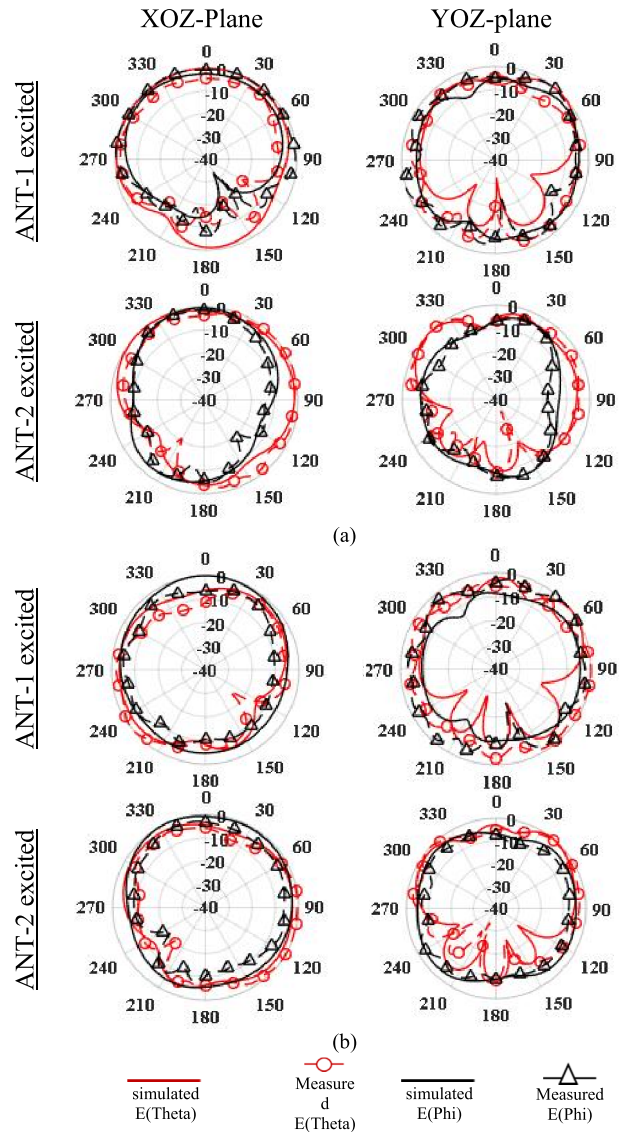
M. A. Fakih *et al.*: Optimization of Efficient Dual Band PIFA System for MIMO Half-Duplex 4G/LTE and Full-Duplex 5G Communications

IEEE *Access*

FIGURE 24. Total efficiency (η_{tot}) of ANT-1 and ANT-2 of the two-PIFA system.

FIGURE 25. Simulated and measured Envelope Correlation (ρ_e).

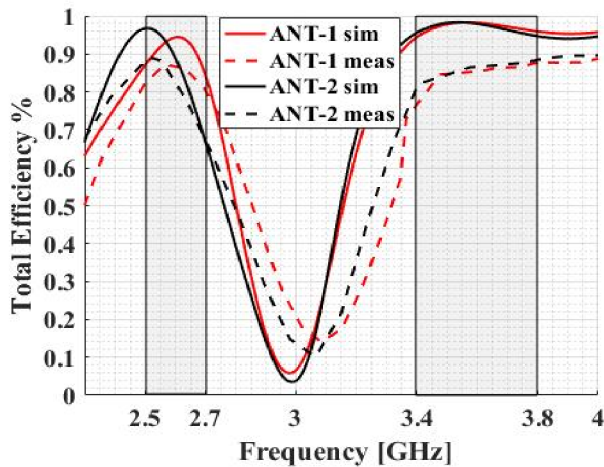The studied efficiency was found to be better than 81% in all the bands. Except [52], none of the previously cited works, where the authors use the neutralization lines technique to have an isolation level of more than 15 dB in the (1.73-2.69 GHz) band, is applied to MIMO communications in mobile terminals. Whereas in our work, first, we used slotting PIFA with parasitic element technique to cover the 4G (2.5-2.7GHz) and 5G (3.4-3.8GHz) bands, and secondly, we achieved a much wider bandwidth up to more than 1GHz including the 5G band thanks to the parasitic element technique. The recorded efficiency is better than 80% in the 2 bands. We have a minimum isolation level of 20 dB for MIMO HD 4G communications and a minimum isolation level of 35 dB for Tx/Rx FD 5G communications by studying and exploiting the characteristic modes of the PCB. Table 2 summarises the comparison between all the cited results.

IV. DIVERSITY CHARACTERIZATION OF MIMO HD 4G ANTENNA SYSTEM PERFORMANCE

First, it should be noted that except the isolation, the performance metrics for 5G FD antenna system are some signal processes or propagation models characterization as the average mobile station downlink experienced rate, the average mobile station uplink experienced rate, the average mobile station sum experienced rate [53]. However, it is not our objective in this work. For 4G, in order to evaluate the diversity performance of the two-PIFA system, the envelope correlation (ρ_e), as well as the diversity system gain (DSG), have been calculated. The envelope correlation is usually calculated from the far-field radiation patterns of the antennas, but it has been demonstrated that for highly efficient antennas, the ρ_e, can be completely determined from the antennas S-parameters [54], where the equation to calculate the ρ_e can be reduced to:

$$\rho_e = \frac{|S_{11}^* S_{12} + S_{12}^* S_{22}|}{(1 - |S_{11}|^2 - |S_{21}|^2)(1 - |S_{22}|^2 - |S_{12}|^2)} \quad (3)$$
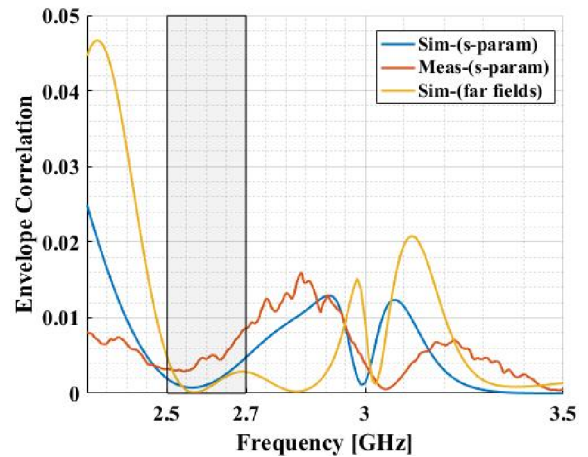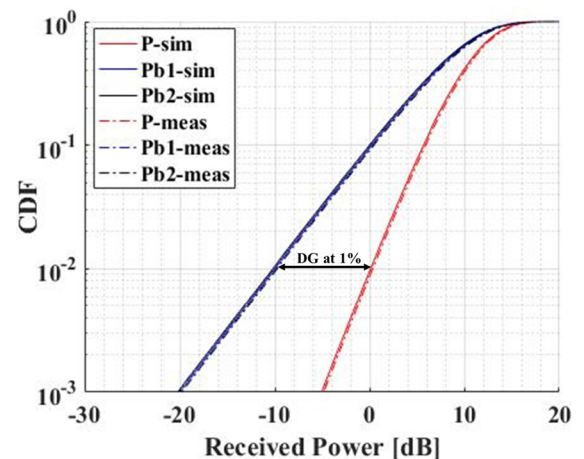
FIGURE 26. Simulated and measured curves of CDF as function of received power by ANT-1, ANT-2 and the combination of the 2 branches at 2.6 GHz.

However, we calculated the envelope correlation by using the two methods (Figure 25). We can see that in the bands where the antennas are well-matched (corresponding to those where the total efficiencies are the highest), the calculated envelope correlation values with the two methods are very close confirming the conditions of use given in [54]. That is why we used the measured S-parameters to calculate the envelope correlation instead of using the measured far-field radiation patterns.

Moreover, we can observe that ρ_e is less than 0.05 in the low band, that is less than the 0.5 reference value generally given for good ρ_e [55]. We notice also that the measured ρ_e by (3) also agrees with the simulated one.

For calculating the DSG, it is first necessary to find the diversity gain (DG) at 2.6 GHz. DG was calculated after plotting the probability density function curves (CDF) of the instantaneous signal to noise ratio (γ) as a function of the received power (x) by each PIFA branch [56], [57].

Figure 26 shows the branch powers *Pb1* and *Pb2* received by ANT-1 and ANT-2 respectively, as well as *P*, the

TABLE 2. Comparison between our work and different similar works of antenna designs over mobile terminals.

Ref	Bands	Method	Efficiency	MIMO Half Duplex	Full Duplex	Isolation technique	Isolation level
[38]	GSM 900 and DSC 1800	Slotted PIFA	Not given	NO	NO	NO	NO
[39]	GSM/PCS and GPS	Slotted PIFA+ Parasitic element	Better 60% in all the bands	NO	NO	NO	NO
[50]	GSM, DCS, PCS, UMTS, WiBro, Bluetooth, SDM-B, WiMAX, WLAN	Slotted PIFA	Better than 79% in all the bands	NO	NO	NO	NO
[51]	WLAN Broadband [2-6 GHz]	PIFA+ Cut etched ground	Not given	NO	NO	NO	NO
[52]	GSM 1800, GSM 1900, UMTS, LTE 2300, LTE 2500, WLAN	IFA antennas	Better than 81% in all the bands	YES [1.73-2.69GHz]	NO	Neutralization lines	>15dB
Our Work	4G LTE 2500, 5G [3.4-3.8GHz]	Slotted PIFA+ Parasitic element	Better than 80% in all the bands	YES [2.5-2.7GHz]	YES [3.4-3.8GHz]	Characteristic modes	HD: >20dB FD: >35dB

combination curve of the two branch powers. The DG_{dB} is calculated at 1% and found to be 10.1 dB. Whereas DSG_{dB} is calculated from (4):

$$DSG_{dB} = DG_{dB} + 10log(\eta_{tot}) \qquad (4)$$

It is found that DSG for ANT-1 is equal to 9.9 dB whereas for ANT-2 it is 9.7 dB. The DG was also calculated from the measurement results and CDF is also plotted in the same Figure 26. DG_{dB} is found to be 10.1 dB where DSG_{dB} is 9.1 dB for ANT-1 and 9.3dB for ANT-2. The difference in the level of DSG_{dB} between simulation and measurement is mainly due to the difference in their corresponding efficiency levels. However, the diversity performance shows that this antenna system is suitable for the intended application. All these results, including the plotted radiation patterns as well as the ρ_e and the DSG meet the requirements of MIMO systems for 4G communications.

V. CONCLUSION
In this work, the design of a dual-band antenna system for future Tx/Rx FD 5G as well as 2×2 HD MIMO 4G communications dedicated for mobile terminals of standard size suitable for nowadays smartphones 140mm × 70mm is presented. The first goal was to provide the two needed frequency bands i.e. the 4G and the 5G bands. Then, the objective was to obtain the best isolation level for the 5G band

using field cancellation technique in order to facilitate the further application of analog and digital cancellation techniques upon fabrication of the whole mobile device. At the same time, a good isolation level for the 4G band for the HD application has to be reached, using only the field cancellation technique and without any reference to other techniques. The best solution consists of having simultaneously the 2 conditions of isolation for the HD MIMO 4G and FD 5G communications without any complications and as less complexity as possible. To achieve this, a characteristic mode analysis was successfully carried out. The results of the work presented in this paper show that our design achieved totally the goal for the HD MIMO of 4G in the low band in terms of matching and bandwidth, with a minimum isolation level of 20 dB. Moreover, we achieved also the whole 400 MHz band coverage as well as a minimum level of 35 dB isolation between the 2 antenna ports and up to more than 60 dB upon the high desired band for FD MIMO of the 5G. The efficiency of our antenna system was also investigated. Indeed, the influence of slot opening position over the PIFA plate on the efficiency of the system was studied. It was shown that the position of the slot is of great importance and has to be taken into consideration when designing the dual-band PIFA. A prototype was fabricated and measured. A good agreement between simulated and measured results was obtained in terms of scattering parameters and total efficiency.

M. A. Fakih *et al.*: Optimization of Efficient Dual Band PIFA System for MIMO Half-Duplex 4G/LTE and Full-Duplex 5G Communications

IEEE*Access*

The diversity and MIMO performance of the system has been also evaluated for the low band. The results showed that our solution is suitable for the intended application. As FD technology over the mobile terminal is of great importance and interest nowadays, the future work will focus mainly on increasing the efficiency and reliability of these systems by trying the use of the MIMO technology for FD MIMO 5G applications.

ACKNOWLEDGMENT

REFERENCES

[1] W. Su, Q. Liu, H. He, and H. Zhang, "A new context awareness scheme for multi-mode mobile terminals in Mobile Internet," in *Proc. IET 3rd Int. Conf. Wireless, Mobile Multimedia Netw.*, Sep. 2010, pp. 95–98.

[2] Y.-L. Ban, C. Li, C.-Y.-D. Sim, G. Wu, and K.-L. Wong, "4G/5G multiple antennas for future multi-mode smartphone applications," *IEEE Access*, vol. 4, pp. 2981–2988, 2016.

[3] M. S. Shinde, A. Nikam, and S. Joshi, "An overview of 5G technology," *Int. Res. J. Eng. Technol.*, vol. 3, no. 4, pp. 2390–2394, 2016.

[4] L. Xu, R. Collier, and G. M. P. O'Hare, "A survey of clustering techniques in WSNs and consideration of the challenges of applying such to 5G IoT scenarios," *IEEE Internet Things J.*, vol. 4, no. 5, pp. 1229–1249, Oct. 2017.

[5] O. M. Haraz, M. M. M. Ali, S. Alshebeili, and A.-R. Sebak, "Design of a 28/38 GHz dual-band printed slot antenna for the future 5G mobile communication Networks," in *Proc. IEEE Int. Symp. Antennas Propag. USNC/URSI Nat. Radio Sci. Meeting*, Jul. 2015, pp. 1532–1533.

[6] Y. Corre, T. Tenoux, J. Stéphan, F. Letourneux, and Y. Lostanlen, "Analysis of outdoor propagation and multi-cell coverage from ray-based simulations in sub-6GHz and mmwave bands," in *Proc. 10th Eur. Conf. Antennas Propag. (EuCAP)*, Apr. 2016, pp. 1–5.

[7] O. M. Haraz, A. Elboushi, S. A. Alsheeili, and A.-R. Sebak, "Dense dielectric patch array antenna with improved radiation characteristics using EBG ground structure and dielectric superstrate for future 5G cellular networks," *IEEE Access*, vol. 2, pp. 909–913, 2014.

[8] D. A. Outerelo, A. V. Alejos, M. G. Sanchez, and M. V. Isasa, "Microstrip antenna for 5G broadband communications: Overview of design issues," in *Proc. IEEE Int. Symp. Antennas Propag. USNC/URSI Nat. Radio Sci. Meeting*, Jan. 2015, pp. 2443–2444.

[9] OFCOM. (Nov. 7, 2017). *Statement-Award-of-the-2.3-and-3.4-GHz-spectrum-bands-Competition-issues-and-auction-regulations.pdf*. Accessed: Dec. 12, 2017. [Online]. Available: https://www.ofcom.org.uk and https://www.ofcom.org.uk/__data/assets/pdf_file/0022/103819/Statement-Award-of-the-2.3-and-3.4-GHz-spectrum-bands-Competition-issues-and-auction-regulations.pdf

[10] W. Hong, "Solving the 5G mobile antenna puzzle: Assessing future directions for the 5G mobile antenna paradigm shift," *IEEE Microw. Mag.*, vol. 18, no. 7, pp. 86–102, Nov. 2017.

[11] L.-Y. Rao and C.-J. Tsai, "8-Loop antenna array in the 5 inches size smartphone for 5G communication the 3.4 GHz-3.6 GHz band MIMO operation," in *Proc. Prog. Electromagn. Res. Symp.*, Toyama, Japan, Aug. 2018, pp. 1995–1999.

[12] S. S. Alja'afreh, Y. Huang, Q. Xu, L. Xing, and O. A. Saraereh, "Dual-element antenna system for hexa-band smartphone MIMO applications," in *Proc. Loughborough Antennas Propag. Conf.*, Loughborough, U.K., Nov. 2017, pp. 1–5.

[13] E. Tsakalaki, E. Foroozanfard, E. de Carvalho, and G. F. Pedersen, "A 2-order MIMO full-duplex antenna system," in *Proc. 8th Eur. Conf. Antennas Propag.*, Apr. 2014, pp. 2546–2550.

[14] D. Korpi, J. Tamminen, M. Turunen, T. Huusari, Y.-S. Choi, L. Anttila, S. Talwar, and M. Valkama, "Full-duplex mobile device: Pushing the limits," *IEEE Commun. Mag.*, vol. 54, no. 9, pp. 80–87, Sep. 2016.

[15] M. G. Sarret, G. Berardinelli, N. H. Mahmood, M. Fleischer, P. Mogensen, and H. Heinz, "Analyzing the potential of full duplex in 5G ultra-dense small cell networks," *EURASIP J. Wireless Commun. Netw.*, vol. 2016, no. 1, p. 284, Dec. 2016.

[16] M. Heino, D. Korpi, T. Huusari, E. Antonio-Rodriguez, S. Venkatasubramanian, T. Riihonen, L. Anttila, C. Icheln, K. Haneda, R. Wichman, and M. Valkama, "Recent advances in antenna design and interference cancellation algorithms for in-band full duplex relays," *IEEE Commun. Mag.*, vol. 53, no. 5, pp. 91–101, May 2015.

[17] B. K. Lau, J. B. Andersen, G. Kristenson, and A. F. Molisch, "Impact of matching network on bandwidth of compact antenna arrays," *IEEE Trans. Antennas Propag.*, vol. 54, no. 11, pp. 3225–3238, Nov. 2006.

[18] A. Diallo, C. Luxey, P. Le Thuc, R. Staraj, and G. Kossiavas, "Enhanced two-antenna structures for universal mobile telecommunications system diversity terminals," *IET Microw. Antennas Propag.*, vol. 2, no. 1, pp. 93–101, Feb. 2008.

[19] H. Li, J. Xiong, and S. He, "A compact planar MIMO antenna system of four elements with similar radiation characteristics and isolation structure," *IEEE Antennas Wireless Propag. Lett.*, vol. 8, pp. 1107–1110, 2009.

[20] C.-Y. Chiu, C.-H. Cheng, R. D. Murch, and C. R. Rowell, "Reduction of mutual coupling between closely-packed antenna elements," *IEEE Trans. Antennas Propag.*, vol. 55, no. 6, pp. 1732–1738, Jun. 2007.

[21] Y. Gao, X. Chen, Z. Ying, and C. Parini, "Design and performance investigation of a dual-element PIFA array at 2.5 GHz for MIMO terminal," *IEEE Trans. Antennas Propag.*, vol. 55, no. 12, pp. 3433–3441, Dec. 2007.

[22] M. A. Abdalla and A. A. Ibrahim, "Compact and closely spaced metamaterial MIMO antenna with high isolation for wireless applications," *IEEE Antennas Wireless Propag. Lett.*, vol. 12, pp. 1452–1455, 2013.

[23] D. Vrba and M. Polivka, "Improvement of the radiation efficiency of the metamaterial zero-order resonator antenna," in *Proc. 14th Conf. Microw. Techn.*, Apr. 2008, pp. 1–3.

[24] A. A. Ibrahim, M. A. Abdalla, A. B. Abdel-Rahman, and H. F. Hamed, "Compact MIMO antenna with optimized mutual coupling reduction using DGS," *Int. J. Microw. Wireless Technol.*, vol. 6, no. 2, pp. 173–180, Apr. 2014.

[25] S. Saini, S. Singh, and N. Kumar, "A review of various planar inverted F antenna (PIFA) structures for wireless applications," *Int. J. Elect. Electron. Eng.*, vol. 1, no. 1, pp. 63–65, 2015.

[26] H. Li, Y. Tan, B. K. Lau, Z. Ying, and S. He, "Characteristic mode based tradeoff analysis of antenna-chassis interactions for multiple antenna terminals," *IEEE Trans. Antennas Propag.*, vol. 60, no. 2, pp. 490–502, Feb. 2012.

[27] H. Li, Z. T. Miers, and B. K. Lau, "Design of orthogonal MIMO handset antennas based on characteristic mode manipulation at frequency bands below 1 GHz," *IEEE Trans. Antennas Propag.*, vol. 62, no. 5, pp. 2756–2766, May 2014.

[28] J. Kim, L. Qu, H. Jo, R. Zhang, and H. Kim, "A MIMO antenna design based on the characteristic mode," *Microw. Opt. Technol. Lett.*, vol. 59, no. 4, pp. 893–898, Apr. 2017.

[29] E. Antonino-Daviu, M. Cabedo-Fabres, M. Gallo, M. Ferrando-Bataller, and M. Bozzetti, "Design of a multimode MIMO antenna using characteristic modes," in *Proc. 3rd Eur. Conf. Antennas Propag.*, Mar. 2009, pp. 1840–1844.

[30] T. Taga, K. Hirasawa, and M. Haneishi, "Analysis of planar inverted-F antennas and antenna design for portable radio equipment," in *Analysis, Design, and Measurement of Small and Low Profile Antennas*, Boston, MA, USA: Artech House, 1992, pp. 161–180.

[31] Cat Phone. *Cat S61 Smartphone*. Accessed: Jun. 27, 2019. [Online]. Available: https://www.catphones.com/en-us/cat-s61-smartphone/

[32] HUAWEI France. *HUAWEI P30 Pro Spécifications du Smartphone*. Accessed: Jun. 27, 2019. [Online]. Available: https://consumer.huawei.com/fr/phones/p30-pro/specs/

[33] Apple (France). *iPhone XR - Caractéristiques Techniques*. Accessed: Jun. 27, 2019. [Online]. Available: https://www.apple.com/fr/iphone-xr/specs/

[34] L. B. Sun, H. Feng, Y. Li, and Z. Zhang, "Compact 5G MIMO mobile phone antennas with tightly arranged orthogonal-mode pairs," *IEEE Trans. Antennas Propag.*, vol. 66, no. 11, pp. 6364–6369, Nov. 2018.

[35] J. Kurvinen, H. Kähkönen, A. Lehtovuori, J. Ala-Laurinaho, and V. Viikari, "Co-designed mm-wave and LTE handset antennas," *IEEE Trans. Antennas Propag.*, vol. 67, no. 3, pp. 1545–1553, Mar. 2019.

[36] R. Addaci, K. Haneda, A. Diallo, P. Le Thuc, C. Luxey, R. Staraj, and P. Vainikainen, "Dual-band WLAN multiantenna system and diversity/MIMO performance evaluation," *IEEE Trans. Antennas Propag.*, vol. 62, no. 3, pp. 1409–1415, Mar. 2014.

[37] P. Ciais, R. Staraj, G. Kossiavas, and C. Luxey, "Design of an internal quad-band antenna for mobile phones," *IEEE Microw. Wireless Compon. Lett.*, vol. 14, no. 4, pp. 148–150, Apr. 2004.

[38] C. W. Chiu and F. L. Lin, "Compact dual-band PIFA with multi-resonators," *Electron. Lett.*, vol. 38, no. 12, pp. 538–540, Jun. 2002.

[39] L. A. Ponce de Leon, "Parasitic element and PIFA antenna structure," in *Proc. IEEE Antennas Propag. Soc. Int. Symp.*, Charleston, SC, USA, Jun. 2009, pp. 1–4.

[40] T. Faradi, A. Diallo, P. Le Thuc, P. Daragon, and R. Staraj, "Design methods for efficient multiband antennas with parasitic elements," in *Proc. 9th Eur. Conf. Antennas Propag. (EuCAP)*, Apr. 2015, pp. 1–4.

[41] M. M. Elsewe and D. Chatterjee, "Characteristic mode analysis of ground plane size in microstrip patch antennas," in *Proc. IEEE Int. Symp. Antennas Propag. (APSURSI)*, Jun./Jul. 2016, pp. 429–430.

[42] A. Bhattacharyya and B. Gupta, "Investigations on effects of finite ground plane on slot antennas using characteristic modes," in *Proc. IEEE Int. Symp. Antennas Propag. USNC/URSI Nat. Radio Sci. Meeting*, Jul. 2017, pp. 169–170.

[43] C. T. Famdie, W. L. Schroeder, and K. Solbach, "Numerical analysis of characteristic modes on the chassis of mobile phones," in *Proc. 1st Eur. Conf. Antennas Propag.*, Nice, France, Nov. 2006, pp. 1–6.

[44] R. & S. G. & C. KG. *R&S ZVRx, R&S ZVCx, R&S ZVM, R&S ZVK Operating Manual*. Accessed: Apr. 25, 2018. [Online]. Available: https://www.rohde-schwarz.com/us/manual/r-s-zvrx-r-s-zvcx-r-s-zvm-r-s-zvk-operating-manual-manuals-gb1_78701-29024.html

[45] B. Xiao, H. Wong, B. Wang, and K. L. Yeung, "Effect of the screen to metal-frame smartphone antennas," in *Proc. Int. Workshop Antenna Technol. (iWAT)*, Miami, FL, USA, Mar. 2019, pp. 29–32.

[46] W. Hong, S. Lim, S. Ko, and Y. G. Kim, "Optically invisible antenna integrated within an OLED touch display panel for IoT applications," *IEEE Trans. Antennas Propag.*, vol. 65, no. 7, pp. 3750–3755, Jul. 2017.

[47] V. Plicanic, B. K. Lau, A. Derneryd, and Z. Ying, "Actual diversity performance of a multiband diversity antenna with hand and head effects," *IEEE Trans. Antennas Propag.*, vol. 57, no. 5, pp. 1547–1556, May 2009.

[48] *N5264A PNA-X Measurement Receiver for Antenna Test | Keysight (formerly Agilent's Electronic Measurement)*. Accessed: Apr. 25, 2018. [Online]. Available: https://www.keysight.com/en/pdx-x201746-pn-N5264A/pna-x-measurement-receiver-for-antenna-test?cc=FR&lc=fre

[49] *StarLab | Antenna Measurement | MVG*. Accessed: Apr. 25, 2018. [Online]. Available: http://www.mvg-world.com/en/products/field_product_family/antenna-measurement-2/starlab

[50] R. A. Bhatti, Y. T. Im, and S. O. Park, "Compact PIFA for mobile terminals supporting multiple cellular and non-cellular standards," *IEEE Trans. Antennas Propag.*, vol. 57, no. 9, pp. 2534–2540, Sep. 2009.

[51] M. Y. Man, R. Yang, Z. Y. Lei, Y. J. Xie, and J. Fan, "Ultra-wideband planar inverted-F antennas with cut-etched ground plane," *Electron. Lett.*, vol. 48, no. 14, pp. 817–818, Jul. 2012.

[52] Y. Wang and Z. Du, "A wideband printed dual-antenna with three neutralization lines for mobile terminals," *IEEE Trans. Antennas Propag.*, vol. 62, no. 3, pp. 1495–1500, Mar. 2014.

[53] O. Al-Saadeh and K. W. Sung, "A performance comparison of in-band full duplex and dynamic TDD for 5G indoor wireless networks," *EURASIP J. Wireless Commun. Netw.*, vol. 2017, no. 1, p. 50, Dec. 2017.

[54] S. Blanch, J. Romeu, and I. Corbella, "Exact representation of antenna system diversity performance from input parameter description," *Electron. Lett.*, vol. 39, no. 9, pp. 705–707, May 2003.

[55] R. G. Vaughan and J. B. Andersen, "Antenna diversity in mobile communications," *IEEE Trans. Veh. Technol.*, vol. 36, no. 4, pp. 149–172, Nov. 1987.

[56] M. Schwartz, W. R. Bennett, and S. Stein, *Communication Systems and Techniques*, vol. 4. Hoboken, NJ, USA: Wiley, 1995.

[57] P.-S. Kildal, K. Rosengren, J. Byun, and J. Lee, "Definition of effective diversity gain and how to measure it in a reverberation chamber," *Microw. Opt. Technol. Lett.*, vol. 34, no. 1, pp. 56–59, 2002.

MOHAMMAD A. FAKIH was born in Majdalzoun, Lebanon, in 1989. He received the bachelor's degree in electronics and the master's degree in signals, telecom, image, and parole processing (STIP) from Lebanese University, in 2010 and 2012, respectively. He taught several classes mainly focusing on electronics and telecom fields with AUCE, Lebanon, for future engineers before joining a joint supervision Ph.D. degree with the University of Saint-Joseph (USJ), Lebanon, and Université Côte d'Azur (UCA), France, from 2016 to 2017. His research interests include small antennas for future 5G mobile terminals, antenna-systems for diversity, and MIMO applications.

ALIOU DIALLO was born in Dakar, Senegal. He received the DEA degree in propagation, telecommunications, and teledetection from the University of Nice Sophia-Antipolis, in 2004, and the Ph.D. degree in electronics with the Laboratory of Electronics, Antennas, and Telecommunications, CNRS, University of Nice Sophia-Antipolis, in 2007, where he is currently an Associate Professor in IUT electrical engineering and a Researcher with the Laboratoire d'Electronique, Antennes et Telecommunications (LEAT), CNRS. His major research area is antenna design and measurements methods for wireless communications and RFID applications, multi-antenna solutions for diversity and MIMO purposes, and implantable antennas. He has presented several conference papers. He was a corecipient of the H. W. Wheeler Award from the IEEE Antennas and Propagation Society for the best application paper of the year 2006 on the transactions on antennas.

PHILIPPE LE THUC was born in Grasse, France, in 1975. He received the Ph.D. and Habilitation à Diriger des Recherches (HDR) degrees in electrical engineering from the University of Nice Sophia-Antipolis (UNS), in 2003 and 2016, respectively, where he has been an Associate Professor, since 2004. He is doing his research with the Laboratory of Electronics, Antennas, and Telecommunications (LEAT), CNRS, University Nice Sophia-Antipolis, where he is the Head of the Conception et Modélisation d'Antennes (CMA) (Antennas Design and Modeling) Research Group. His research interests include design of small antennas, antenna-systems for diversity, and MIMO applications and antennas associated with sensors for biomedicine and radio-frequency identification. He is also a Reviewer of the IEEE Transactions on Antennas and Propagation.

ROBERT STARAJ was born in Antibes, France, in 1965. He received the Ph.D. degree in electronics from University of Nice-Sophia Antipolis (UNS), France, in 1992. In 1993, he integrated the Engineering School Ecole Supérieure d'Ingénieurs de Nice-Sophia Antipolis (ESINSA) and the Laboratory of Electronics, Antennas, and Télécommunications (LEAT), CNRS, as an Assistant Professor. Since 2003, he has been a Full Professor with Polytech'Nice-Sophia (Ecole Polytechnique de l' Université de Nice-Sophia) and the in charge of the telecommunications and networks specialty with the Electronics Department, University of Nice Sophia-Antipolis. He was also the Director of the GDR Ondes-CNRS French National Research Group on Waves, from 2014 to 2017 and an Assistant Director of the LEAT. After being the Head of the Conception et Modélisation d'Antennes (CMA) Research Group (Antennas Design and Modeling), LEAT, for several years, he is currently the Director. His research interests include printed antennas and arrays, active, integrated, adaptative, and miniature multistandard antennas for wireless, RFID, MIMO systems, and biomedical applications.

M. A. Fakih *et al.*: Optimization of Efficient Dual Band PIFA System for MIMO Half-Duplex 4G/LTE and Full-Duplex 5G Communications

IEEE *Access*

OUMAR MOURAD was born in Lebanon, in 1987. He received the bachelor's degree in electronics from Lebanese University, in 2008, and the master's and Ph.D. degrees in electronics from the University Nice Sophia Antipolis (UNS), France, in 2010 and 2014, respectively. He currently teaches in several universities such as Université Saint-Joseph (USJ), USEK, UA, and Lebanese University, where he mainly focuses on electronics fields for future engineers and physicists. His research interests include antennas, RFID, electronics, printed electronics materials, and RF communications.

ELIAS A. RACHID (SM'09) was born in Lebanon, in 1966. He received the M.S. degree in telecommunications engineering from the University of Saint-Joseph (USJ) (Ecole Supérieure d'Ingénieurs de Beyrouth ESIB), Beirut, Lebanon, in 1990, and the Ph.D. degree in electronics and signal processing (microwave) from University Marnes La Vallée, Paris, and the National Institute of Telecom Evry, France, in 2004. He joined the ESIB, in 1990, where he is a Full Professor and the Director of the CINET Center of Electrical and Telecommunications Industries (CINET), ESIB, Université Saint-Joseph. His research interests include electromagnetic scattering and diffraction, ray-tracing methods, and the areas of printed antennas and electromagnetic pollution.

• • •